MITSUBISHI ELECTRIC RESEARCH LABORATORIES
http://www.merl.com

Model-Based Analysis and Quantification of Bearing Faults in Induction Machines

Zhang, Shen; Wang, Bingnan; Kanemaru, Makoto; Lin, Chungwei; Liu, Dehong; Habetler, Thomas

TR2020-059 May 14, 2020

Abstract

The detection of rolling-element bearing fault can be accomplished by monitoring and interpreting a variety of signals, including the vibration, the acoustic noise, and the stator current. The existence of a bearing fault as well as its specific fault type can be readily determined by performing frequency spectral analysis on the monitored signals with various signal processing techniques. However, this traditional approach, despite being simple and intuitive, is not able to identify the severity of a bearing fault in a quantitatively manner. Moreover, it is oftentimes tedious and time-consuming to apply this approach to electric machines with different power ratings, as the bearing fault threshold values need to be manually calibrated for each motor running at every possible speed and carrying any possible load. This paper thus proposes a quantitative approach to estimate the bearing fault severity based on the air gap displacement profile, which is reconstructed from the mutual inductance variation profile estimated from a quantitative electrical model that takes the stator current as input. In addition, the accuracy of the developed electrical model and the estimated bearing fault severity are validated by the simulation and experimental results, and the explicit air gap variation profile is reconstructed with the superposition of multiple Fourier Series terms estimated from the stator current via the proposed scheme. The proposed method offers a quantitative and universal bearing fault indicator for induction machines with any power ratings and operating under any speed and load conditions.

IEEE Transactions on Industry Applications

Model-Based Analysis and Quantification of Bearing Faults in Induction Machines

Shen Zhang, *Member, IEEE,* Bingnan Wang, *Senior Member, IEEE,* Makoto Kanemaru, Chungwei Lin, Dehong Liu, *Senior Member, IEEE,* Masahito Miyoshi, Koon Hoo Teo, *Member, IEEE,* and Thomas G. Habetler, *Fellow, IEEE*

***Abstract*—The detection of rolling-element bearing fault can be accomplished by monitoring and interpreting a variety of signals, including the vibration, the acoustic noise, and the stator current. The existence of a bearing fault as well as its specific fault type can be readily determined by performing frequency spectral analysis on the monitored signals with various signal processing techniques. However, this traditional approach, despite being simple and intuitive, is not able to identify the severity of a bearing fault in a quantitatively manner. Moreover, it is oftentimes tedious and time-consuming to apply this approach to electric machines with different power ratings, as the bearing fault threshold values need to be manually calibrated for each motor running at every possible speed and carrying any possible load. This paper thus proposes a quantitative approach to estimate the bearing fault severity based on the air gap displacement profile, which is reconstructed from the mutual inductance variation profile estimated from a quantitative electrical model that takes the stator current as input. In addition, the accuracy of the developed electrical model and the estimated bearing fault severity are validated by the simulation and experimental results, and the explicit air gap variation profile is reconstructed with the superposition of multiple Fourier Series terms estimated from the stator current via the proposed scheme. The proposed method offers a quantitative and universal bearing fault indicator for induction machines with any power ratings and operating under any speed and load conditions.**

***Index Terms*—Bearing fault, fault severity, analytical model, mutual inductance variation, air gap displacement.**

I. Introduction

Induction machines are broadly used in various industry applications including pumps, chemical, petrochemical, and electrified transportation systems, etc. In many scenarios, these machines are operated at some unfavorable conditions, such as high ambient temperature, high moisture and overload, which can eventually result in motor malfunctions that lead to high maintenance costs and severe financial losses due to unexpected downtime [1]–[3].

The malfunction of induction machines can be generally attributed to various faults of different categories, which includes the drive inverter failure, the stator winding insulation breakdown, the broken rotor bar fault, as well as the bearing fault and the air gap eccentricity. Several surveys investigating the likelihood of induction machine failures conducted by the IEEE Industry Application Society (IEEE-IAS) [4]–[6] and the Japan Electrical Manufacturers' Association (JEMA) [7] reveal that the bearing fault is the most common fault type that accounts for 30% to 40% of all of the failures. Therefore, there is a strong demand for developing an accurate fault detection algorithm to identify the presence of a bearing fault.

The structure of a rolling-element bearing is illustrated in Fig. 1, which contains the outer race mounted on the motor cap, the inner race to hold the motor shaft, the ball or rolling element and the cage for restraining the relative locations of the many rolling elements. Four common scenarios of misalignment that may cause bearing failures are demonstrated in Fig. 1(a) to (d). Bearing fault detection has attracted the attention of many researchers and engineers from both mechanical engineering and electrical engineering. Specifically, this problem has been approached by interpreting a variety of signals, including vibration, acoustic noise, and stator current. In addition, some new and emerging methods for bearing fault detection include the sensor fusion of vibration and acoustic signals [8], thermal-imaging [9], as well as various machine learning algorithms [10]–[13] that require a large amount of input signals as the training set. On a fundamental basis, the existence of a bearing fault as well as its specific fault type can be readily determined by performing frequency spectral analyses on the monitored signal at the characteristic fault frequency, which can be calculated by a well-established mechanical model [14] that depends on the motor speed, the bearing geometry, the specific location of a bearing defect, etc.

Some straightforward bearing fault detection methods are based on extracting the fault signature from the vibration [15], [16] and acoustic noise [17], [18] signals. Usually measured in the form of displacement, speed, or acceleration, the vibration signal is a direct mechanical response of the impact between rolling elements and inner/outer raceways if some defects or wears have been developed due to fatigue or excessive radial load. Similarly, certain high-frequency ultrasonic acoustic noise signal is also generated in this process and can be used to monitor various bearing defects. After performing the frequency spectral analysis, a bearing fault can be detected by comparing the result against a pre-stored spectrum of a healthy bearing conditions at certain rotating speed and load.

However, the accuracy of bearing fault diagnostics based on vibration or acoustic signals can be influenced by background

S. Zhang, and T. G. Habetler are with the School of Electrical and Computer Engineering, Georgia Institute of Technology, Atlanta, GA 30332, USA (e-mail: shenzhang@gatech.edu, thabetler@ece.gatech.edu).

B. Wang, C. Lin, D. Liu and K. H. Teo are with the Mitsubishi Electric Research Laboratories, 201 Broadway, Cambridge, MA 02139, (e-mail: bwang@merl.com, clin@merl.com, liudh@merl.com, teo@merl.com).

M. Kanemaru and M. Miyoshi are with the Advanced R&D Center, Mitsubishi Electric Corporation, Amagasaki, Japan (e-mail: Kanemaru.Makoto@cw.MitsubishiElectric.co.jp, Miyoshi.Masahito@ay.MitsubishiElectric.co.jp).

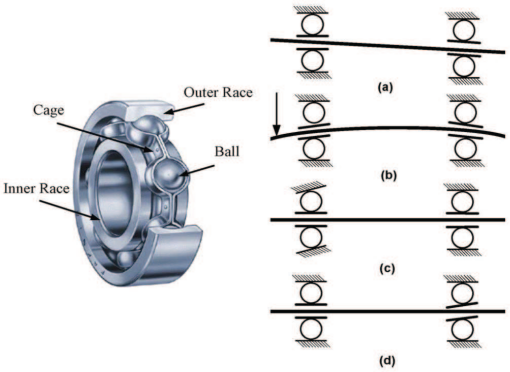

Fig. 1. Structure of a rolling-element bearing with four types of bearing misalignment: (a) misalignment (out-of-line), (b) shaft deflection, (c) cocked or tilted outer race and (d) cocked or tilted inner race [45].

noise due to mechanical excitation from an external source, while its sensitivity is also subject to change based on sensor mounting positions that usually come with spatial constraints in a highly-compact design. Therefore, a popular alternative approach is to analyze the induction machine stator current [19]–[24], which is measured in most motor control centers or motor drives and thus would not bring extra device or installation costs.

Despite many advantages such as economic savings and simple implementation, accomplishing bearing fault detection with motor current signature analysis (MCSA) can encounter many practical issues. For example, the magnitude of stator currents at bearing fault signature frequencies can vary at different loads [25], different speeds, and different power ratings of the motor itself, thus bringing challenges to identify threshold values of the stator current to trigger the fault alarm at an arbitrary operating condition. For example, it has been reported in [26] that fault misdetection can happen due to an increase in load current. Therefore, a thorough and systematic testing is usually required while the bearing is still at the healthy state, and this healthy data need to be collected and categorized at different load conditions [26]. In patent US5726905 [25], the measurement of motor current is more rigorously divided into statistically homogenous segments representative of respective load patterns in good (healthy) operating modes.

However, this so-called "Learning Stage" or intensive data acquisition/storage is required for most existing MCSA methods up to date, which sometimes require heavy dataset to detect even nonfatal fault. To make it worse, while bearing fault detection based on this commissioning manner may perform well on motors normally running at a few operating conditions, it can become tedious, exhaustive, or even infeasible for applications where motors do not have fixed operating points, such as the electric vehicle. In addition, the detection of bearing faults with conventional methods is mostly performed in a qualitative manner, whereas the exact faulty condition cannot be quantified. Therefore, a universal, accurate and quantitative method is desired for detecting bearing faults in induction motors at any operating condition.

It is generally believed that a bearing fault has two major effects on the motor performance [20], [21]: the introduction of 1) load torque variations and 2) a periodic radial rotor movement. At the incipient stage of a bearing fault, the effect of load torque variations on electrical signals is largely suppressed due to the large inertia of the motor-load system, and thus the motor speed oscillation can be often neglected. On the other hand, a periodic radial movement of the rotor can be considered as a form of vibration that induces a periodic change of the air gap length, which further leads to a periodic change of the motor mutual inductance profile and affect the stator current. However, it has been recognized in the literature that the exact physical model that links vibrations to motor current spectral components is unclear [16], [27] and still requires extensive attention [28].

In this context, this paper seeks to bridge the gap between radial vibrations and stator current spectral components. Specifically, it proposes a novel quantitative method to estimate the bearing fault severity in terms of radial air gap displacement using the developed analytical equations of an induction machine with bearing faults [29]. The model is based on the transient partial differential equation of an induction machine and describes a relationship between the mutual inductance variation induced by a bearing fault and its corresponding change of the stator current. Using either the first order or the superposition of a series of Fourier terms, the magnitude or the cumulative profile of the mutual inductance in the time domain can be revealed and reconstructed. Then, a transfer function is adopted to link the mutual inductance variation and the air gap length variation, which is defined as the indicator of the bearing fault severity in this study. Existing literature on bearing fault severity estimation can be broadly categorized into data-driven approaches and model-based approaches. A large portion of the existing work falls into data-driven approaches, where fault features can be manually or automatically extracted from data collected during faulty conditions to train a statistical or machine learning algorithm [30], such as the wavelet packet energy entropy [31], the adaptive neural fuzzy inference system [32], and convolutional neural networks [33], etc. While these methods can be accurate and effective, a large amount of data is typically needed *a priori* to train these algorithms, and this training process needs to be repeated for each different motor-bearing setup.

The model-based methods, on the other hand, are built upon solid understandings of the physical nature of bearing defects and their influences on various mechanical and electrical signals [34]. In [35], a comprehensive nonlinear dynamic model based on vibration mechanism is developed to estimate the size and severity of a bearing defect. However, this mechanical model still requires vibration signals despite its high-fidelity and good accuracy, making it necessary to install additional accelerometers to the system. While a preliminary work is presented in [28] that attempts to use the stator current for estimating the bearing fault severity, it has created a mapping from the bearing defect to stator current obtained through experiments, rather than establishing a solid analytical model that links the mechanical vibration to the dynamics of electric machines. Additionally, there would be different mappings for

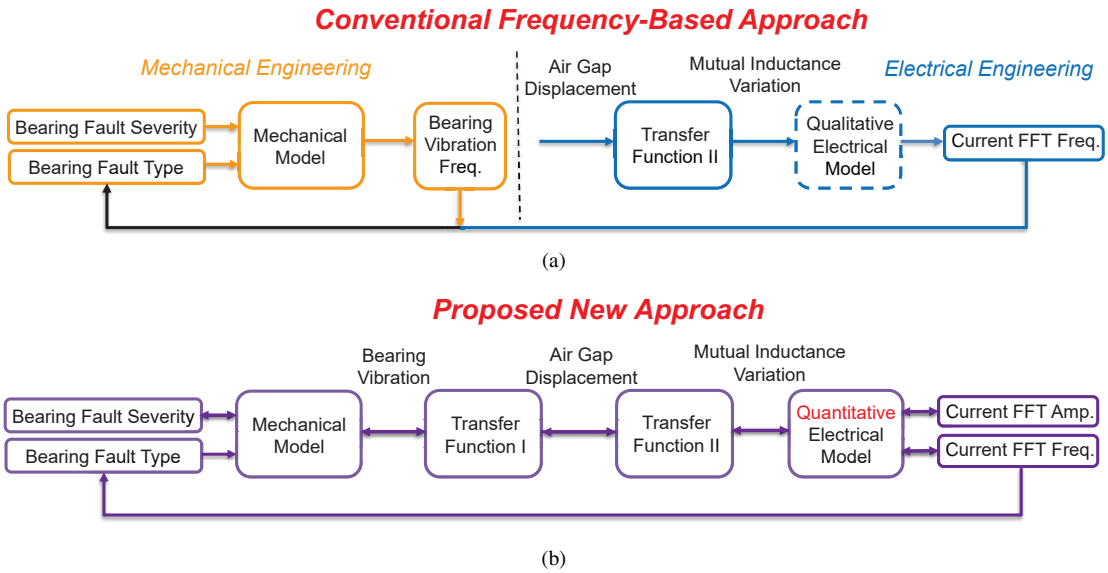

Fig. 2. Flow diagrams of bearing fault diagnostics: (a) the traditional approach and (b) the proposed new vision.

different motor-bearing setups that run at arbitrary speed and load conditions.

Therefore, this paper proposes a model-based approach that quantifies the bearing fault severity using stator current, which has an advantage over data-driven approaches as it does not require a large amount of faulty data collected *a priori* to train the employed algorithm. In addition, it is more convenient and cost-effective than vibration model based approach, which requires the installation of additional accelerometers, while in many applications the current sensors have been already installed for motor control purposes. Moreover, the proposed model is able to identify the fault severity of bearings on induction machines that run at any speed and load conditions.

II. A New Vision for Bearing Fault Detection

A. Traditional Bearing Fault Detection Technique

In this section, the traditional approach for bearing fault detection and its limitations will be presented, then a new vision is proposed to come up with a quantitative and universal fault indicator, as well as the potential to reveal both the size and the location of a specific bearing defect.

Fig. 2(a) is a flow diagram of procedures undertaking by mechanical and electrical engineers to detect the presence of a bearing fault and its fault type. From the physical point of view, when a bearing fault appears on certain locations that characterizes its bearing fault type with a certain fault severity, some periodic vibration pulses will be generated as a result of the impact among the rolling element, the bearing raceway, and the cage with a characteristic frequency f_c depending on the fault type, which includes a cage defect hitting the inner/outer bearing raceways, an inner/outer raceway defect hitting the rolling elements, and a rolling element defect hitting both the inner and outer raceways. For the five fault types mentioned above, f_c takes the following expressions:

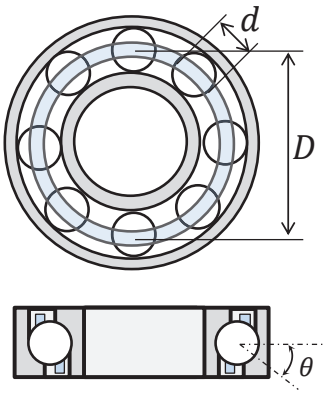

Fig. 3. A rolling-element bearing illustrating its geometric parameters.

$$\text{Cage defect hits outer race:} \quad f_{co} = \frac{f_r}{2}\left(1 - \frac{d}{D}\cos\theta\right)$$

$$\text{Cage defect hits inner race:} \quad f_{ci} = \frac{f_r}{2}\left(1 + \frac{d}{D}\cos\theta\right)$$

$$\text{Outer race defect hits balls:} \quad f_o = N_b\frac{f_r}{2}\left(1 - \frac{d}{D}\cos\theta\right)$$

$$\text{Inner race defect hits balls:} \quad f_i = N_b\frac{f_r}{2}\left(1 + \frac{d}{D}\cos\theta\right)$$

$$\text{Ball defect hits both races:} \quad f_b = \frac{D}{d}f_r\left(1 - \frac{d^2}{D^2}\cos^2\theta\right)$$

where the number of balls is denoted as N_b, the ball diameter is d, and the pitch or cage diameter is D. The point of contact between the ball and the raceway is characterized by the contact angle θ, as shown in Fig. 3, and f_r is the mechanical frequency of the rotor.

The mechanical mechanism for generating such vibrations can be formulated with either the analytical equation [36]–[39] or the finite element analysis [40]–[44]. While the relationship

between a bearing fault type and its associated vibration frequency is already well-defined in [14], mechanical engineers have been investigating how bearing defects of different width, depth and at different location would impact the shape and intensity of the vibration signal.

Specifically, the vibration from a bearing fault is an indicator of a periodic air gap displacement in the radial direction, which further causes a periodic variation of the mutual inductance L_m of the same characteristic fault frequency f_c characterized by the Transfer Function II. Due to this mutual inductance change, the frequency component of the stator current at $|f_s \pm n \cdot f_c|$ will be present in response to the bearing fault, where f_s is the fundamental frequency of the input voltage. This mechanism can be formulated as a Qualitative Electrical Model, e.g., [19], [21], which can identify the presence of a bearing fault and its specific fault type. This traditional approach, however, is not able to predict the size or severity of such a bearing fault, either from the vibration signal or from the stator current signal.

B. A New Vision of Bearing Fault Detection

This section presents a new vision for bearing fault detection to reveal both the bearing fault type and its fault severity with the integration of both electrical and mechanical models, as illustrated in Fig. 2(b). The input would be the stator current amplitude of electrical characteristic fault frequency $|f_s \pm n f_c|$ determined by the bearing geometry and the instantaneous motor speed [14]. Then the mutual inductance variation profile can be reconstructed with the developed Quantitative Electrical Model of induction machines with bearing faults, which can be further transformed into an air gap displacement signal with a Transfer Function II. With the knowledge of bearing mounting positions on the shaft relative to the center of the air gap, the vibration intensity at bearing locations can be inferred by a Transfer Function I based on either complex beam theories or a simple linear decay function of mechanical vibrations. The Mechanical Model can be constructed as a direct analytical relationship between the vibration signal pattern and the bearing fault size/severity [36]–[39], or via reverse mapping with finite element analysis [40]–[44] for bearing defects with irregular shapes, since their corresponding analytical equations would be difficult to formulate. Similarly, the type of a bearing fault can be directly inferred from its associated fault current frequency.

Compared to the conventional approach illustrated in Fig. 2(a), this new vision is an integrated approach of mechanical and electrical modeling. While the conventional approach can only determine the type of a bearing fault, this new vision can also estimate its actual fault severity by estimating the air bap length variation. This approach is feasible due to the fact that the vertical position of the shaft will change when the defect hits the rolling element or the bearing raceways. In addition, the larger the size (severity) of the defect, the larger the shaft displacement. Therefore, the magnitude of the air gap variation profile can be used to indicate the size (severity) of a bearing defect, and the percentage of the maximum displacement with regard to the nominal air gap length can be used to quantify such a fault severity.

This paper fulfills the electrical part of this vision, namely the Quantitative Electrical Model and Transfer Functions I & II, and the bearing fault severity is quantified in terms of the normalized air gap displacement estimated from the stator current. The final goal of this vision, however, is to predict the size and location of a defect inside a bearing by measuring and interpreting the stator current.

III. The Quantitative Electrical Model Estimating the Mutual Inductance Variation

The Quantitative Electrical Model is developed to estimate the mutual inductance variation from the input stator current. The response to bearing faults can be considered as a combination of mutual inductance variations (including stator-to-stator, stator-to-rotor, and rotor-to-rotor) due to the induced dynamic air gap eccentricity and load torque oscillations that would further lead to speed oscillations. For most induction machine setups, however, the system inertia is large enough to suppress small speed oscillations, and thus the effect of load torque oscillations is neglected in the later model development stage, which assumes the bearing fault is still at its incipient stage.

The mathematical model for squirrel-cage induction machines in the stationary reference frame with a rotational speed of 0 can be expressed as

$$\begin{cases} \mathbf{u_{ds}} = R_s \mathbf{i_{ds}} + p\lambda_{\mathbf{ds}} \\ \mathbf{u_{qs}} = R_s \mathbf{i_{qs}} + p\lambda_{\mathbf{qs}} \\ 0 = R_r \mathbf{i_{dr}} + p\lambda_{\mathbf{dr}} + \omega_r \lambda_{\mathbf{qr}} \\ 0 = R_r \mathbf{i_{qr}} + p\lambda_{\mathbf{qr}} - \omega_r \lambda_{\mathbf{dr}} \end{cases} \tag{1}$$

$$\begin{cases} \lambda_{\mathbf{ds}} = L_s \mathbf{i_{ds}} + L_m \mathbf{i_{dr}} \\ \lambda_{\mathbf{qs}} = L_s \mathbf{i_{qs}} + L_m \mathbf{i_{qr}} \\ \lambda_{\mathbf{dr}} = L_m \mathbf{i_{ds}} + L_r \mathbf{i_{dr}} \\ \lambda_{\mathbf{qr}} = L_m \mathbf{i_{qs}} + L_r \mathbf{i_{qr}} \end{cases} \tag{2}$$

where $\mathbf{u}$ is the input voltage, R and L are the motor resistance and inductance, ω_r is the electrical rotor speed, λ is the flux linkage, p is the differential operator, subscripts d and q represent the direct and quadrature axes, and subscripts s, r and m denote the stator, rotor, and their mutual electromagnetic parameters. The parameters in bold representations are vectors with both an amplitude (with a phasor) and a rotational speed. By defining the phasor of $\mathbf{u_{ds}}$ to be zero, i.e., $\varphi_{ds} = 0$, for example, we'll have $\mathbf{u_{qs}} = |u|e^{-i\varphi_{qs}}e^{-i\omega_s t} = u_{qs}e^{-i\omega_s t}$, where $\mathbf{u_{qs}}$ is the vector expression of the stator voltage in the q-axis, φ_{qs} is its phasor, $|u|$ is the magnitude of the stator voltage without the phasor, $u_{qs} = |u|e^{-i\varphi_{qs}}$ is the magnitude with the phasor, and ω_s is the synchronous speed.

Then a matrix form of the above equation can be written in (3), where U is the input matrix, $P^{(0)}$ is the parametric matrix for a healthy induction machine, $X^{(0)}$ is the response matrix in the steady-state containing all of the state variables of the stator and rotor flux linkages and currents, and K is the coefficient matrix for the first-order derivatives of state X.

Consider a bearing fault that leads to a periodic air gap variation, which further leads to a periodic change of the

stator-to-stator, stator-to-rotor, and the rotor-to-rotor mutual inductance. While the pattern of the periodic air gap variation can be decomposed into a series of Fourier Series, the simplest form is to only take its fundamental frequency component at f_c and its magnitude as ΔL_m. The model can be formulated with this assumption first, and the final result of mutual inductance variation would be the superposition of all of the harmonic contents derived in the same manner from this model. In this scenario, the updated mutual inductance becomes

$$L_m^{new} = L_m + \Delta L_m \cos(\omega_c t) \tag{4}$$

Then the new form of the parameter matrix P is

$$\begin{cases} P = P^{(0)} + \Delta\widetilde{P}(t) \\ \Delta\widetilde{P}(t) = \Delta L_m \cos(\omega_c t) \cdot M \\ M = \left[\begin{array}{c|cc} \mathbf{0} & \mathbf{0} & \\ \hline \mathbf{0} & \mathbf{I} & \mathbf{I} \\ & \mathbf{I} & \mathbf{I} \end{array}\right] \end{cases} \tag{5}$$

When this change is applied to the induction motor equation in the d-q axis, all inductance variables will contain the bearing fault frequency f_c term and the DC term L_m, which are later multiplied with the current terms to calculate the flux linkage. Assume initially these current terms only contain the motor synchronous frequency f_s term, the multiplication of f_c and f_s frequency terms would yield both f_s+f_c and f_s-f_c terms. Almost instantly afterward, both the f_s+f_c and f_s-f_c terms will show up in the stator and rotor current due to Eqn. (1). Therefore, in the frequency domain, the complete induction machine equation under mutual inductance change can be written as Eqn. (6), where superscripts "+" and "−" represent variables at frequencies f_s+f_c and f_s-f_c. Therefore, X^+ and X^- are the state variable X at frequencies f_s+f_c and f_s-f_c, with the corresponding angular speeds of $\omega^+ = 2\pi(f_s+f_c)$ and $\omega^- = 2\pi(f_s-f_c)$.

Additionally, based on the superposition theorem, we can separate an equation involving multiple frequencies into multiple equations at their own frequency domains. Then the complete solutions X^+ and X^- for a faulty frequency pair f_s+f_c and f_s-f_c can solved in two separate equations as

$$\begin{cases} \left(P^{(0)} - i\omega^+ K\right) X^+ + \dfrac{\Delta L_m}{2} M X^{(0)} = 0 \\ \left(P^{(0)} - i\omega^- K\right) X^- + \dfrac{\Delta L_m}{2} M X^{(0)} = 0 \end{cases} \tag{7}$$

where $X^{(0)}$ is the solution of

$$\left(P^{(0)} - i\omega_s K\right) X^{(0)} + \frac{\Delta L_m}{2} M(X^+ + X^-) = U \tag{8}$$

It can be observed that equations (7) and (8) are coupled in terms of X^+ and X^- even at different frequency domains. However, the $(X^+ + X^-)$ term is generally way smaller than $X(0)$ (the stator current at fault frequency pairs $f_s \pm f_c$ can be around 40 to 50 dB smaller than the rated current at f_s). Additionally, it is also getting multiplied by ΔL_m, and this ΔL_m term is also smaller when compared to their corresponding elements in matrix $(P(0) - i\omega_s K)$, where these elements can be the stator inductance L_s, the rotor inductance L_r, and the mutual inductance L_m at the healthy condition. Therefore, the product of ΔL_m and $(X^+ + X^-)$ can be viewed as a second-order small-signal term, which can be safely neglected. Therefore, equation (8) can be updated into

$$\left(P^{(0)} - i\omega_s K\right) X^{(0)} = U \tag{9}$$

Since the measured stator current is contained in the state variable matrix X, and matrix $(P^{(0)} - i\omega^{\pm} K)$ is invertible under the context of induction machines, thus the corresponding rows of the stator current in matrix $(P^{(0)} - i\omega^{\pm} K)^{-1} M X^{(0)}$ can be extracted as A^+ and A^- for angular speeds ω^+ and ω^-. Additionally, the following results can be obtained since ΔL_m is a scalar

$$\begin{cases} |\Delta I^+| = |A^+| \cdot \dfrac{\Delta L_m}{2} \\ |\Delta I^-| = |A^-| \cdot \dfrac{\Delta L_m}{2} \end{cases} \tag{10}$$

in which $|\Delta I^+|$ and $|\Delta I^-|$ are magnitudes of the faulty stator current for an electrical fault frequency pair f_s+f_c and f_s-

$$\underbrace{\begin{bmatrix} u_{ds} \\ u_{qs} \\ 0 \\ 0 \\ 0 \\ 0 \\ 0 \\ 0 \end{bmatrix}}_{U} \cdot e^{-i\omega_s t} = \underbrace{\begin{bmatrix} 0 & 0 & 0 & 0 & R_s & 0 & 0 & 0 \\ 0 & 0 & 0 & 0 & 0 & R_s & 0 & 0 \\ 0 & 0 & 0 & \omega_r & 0 & 0 & R_r & 0 \\ 0 & 0 & -\omega_r & 0 & 0 & 0 & 0 & R_r \\ -1 & 0 & 0 & 0 & L_s & 0 & L_m & 0 \\ 0 & -1 & 0 & 0 & 0 & L_s & 0 & L_m \\ 0 & 0 & -1 & 0 & L_m & 0 & L_r & 0 \\ 0 & 0 & 0 & -1 & 0 & L_m & 0 & L_r \end{bmatrix}}_{P^{(0)}} \cdot \underbrace{\begin{bmatrix} \lambda_{ds} \\ \lambda_{qs} \\ \lambda_{dr} \\ \lambda_{qr} \\ i_{ds} \\ i_{qs} \\ i_{dr} \\ i_{qr} \end{bmatrix}}_{X^{(0)}} \cdot e^{-i\omega_s t} + \underbrace{\left[\begin{array}{c|c} \mathbf{I} & \mathbf{0} \\ \hline \mathbf{0} & \mathbf{0} \end{array}\right]}_{K} \cdot p \left\{ \begin{bmatrix} \lambda_{ds} \\ \lambda_{qs} \\ \lambda_{dr} \\ \lambda_{qr} \\ i_{ds} \\ i_{qs} \\ i_{dr} \\ i_{qr} \end{bmatrix} \cdot e^{-i\omega_s t} \right\} \tag{3}$$

$$\begin{aligned} &\left[P^{(0)} + \frac{\Delta L_m}{2}(e^{i\omega_c t} + e^{-i\omega_c t}) M\right] \cdot (X^{(0)} e^{-i\omega_s t} + X^+ e^{-i\omega^+ t} + X^- e^{-i\omega^- t}) \\ &+ \left[(-i\omega_s) K X^{(0)} e^{-i\omega_s t} + (-i\omega^+) K X^+ e^{-i\omega^+ t} + (-i\omega^-) K X^- e^{-i\omega^- t}\right] = U \cdot e^{-i\omega_s t} \end{aligned} \tag{6}$$

f_c. The task for the next stage is to extract actual values or any form of combinations of $|\Delta I^+|$ and $|\Delta I^-|$ to the best possible accuracy via signal processing techniques to estimate the mutual inductance variation ΔL_m.

IV. Signal Processing Techniques

A. Technical Challenges

Unfortunately, accurately extracting the faulty stator current at the bearing fault characteristic frequency is not simple, as there are some technical challenges that affect the performance of conventional signal processing techniques.

1) Irrational fault frequency f_c: The bearing characteristic fault frequency f_c depends on both the bearing geometry and the motor speed ω_r, which can be an arbitrary value for mains-fed induction machines depending on the load condition. Moreover, it is almost certain that the fault frequency f_c is not an integer, but rather an irrational number. As a result, the most commonly used Fast Fourier Transform (FFT) cannot be readily used, as the FFT window length (number of sampling points) need to be adjusted to be an integer multiple of f_c, otherwise the accurate values of this frequency component cannot be extracted. A preliminary study performed by the authors suggests the FFT error can be well over 30% if the FFT window length is not selected based on the above criterion, even if the window length is sufficiently long.

2) Real-time implementation: Although for many applications it would be acceptable to perform a single bearing fault detection during an extended period of time, i.e., one to a few hours. It would be desirable if the proposed signal processing technique is able to reveal accurate faulty current components in a real-time manner, and thus the bearing fault can be also monitored in real-time, which would be beneficial for some safety-critical applications, i.e., electric vehicles.

B. The Proposed Method – Software based Notch Filter

Taking the above challenges into consideration, an alternative approach based on a "software-based notch filter" is proposed in Fig. 4. While many other signal processing techniques may be used to fulfill the same purpose, i.e., compressive sensing [46], it is envisioned that the proposed method is simple, accurate, and can be readily embedded in a controller or a digital signal processor for the purpose of real-time monitoring.

A flow diagram illustrating the process to extract the faulty current at the electrical characteristic fault frequency $(f_s \pm n f_c)$ is shown in Fig. 4, which is then fed into the Quantitative Electrical Model for estimating the mutual inductance variation ΔL_m. The proposed method takes direct measurements of stator current in a time domain, and for an induction machine with n phases, only $n-1$ phase current measurements are required, since the additional phase current can be calculated with Kirchhoff's current law. Then the Park Transformation is applied on the measured stator currents to obtain the direct and quadrature axis current in the synchronous reference frame, and thus the largest fundamental AC component in the stator current is transformed into a DC value, which can be easily filtered out by performing low-pass filtering and subtraction,

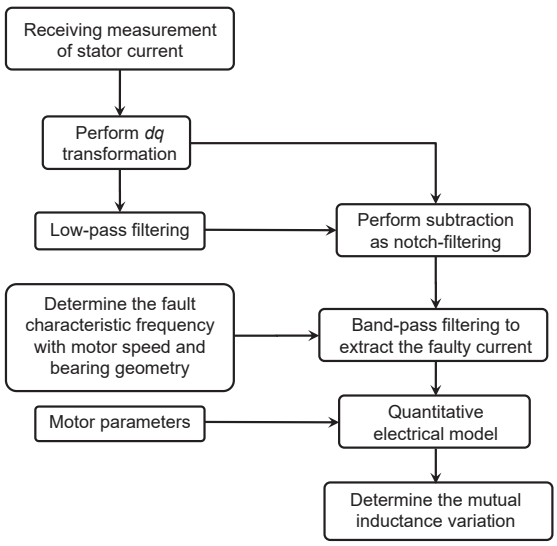

Fig. 4. Proposed signal processing technique for extracting the sum of the stator current component of the faulty frequency pairs for estimating the mutual inductance variation.

which will be referred to as "software-based notch filtering" for the rest of this paper. This algorithm then determines the electrical characteristic fault frequency pairs $(f_s \pm n f_c)$ using the bearing geometry data and the real-time motor speed. Then band-pass filters are designed to extract these faulty current from the stator current signal. Eventually, the absolute value of the result from band-pass filtering will be taken as the final faulty current.

Intuitively, the electrical bearing fault frequencies can be transformed to $\pm f_c$ from $(f_s \pm f_c)$ after taking the Park transformation, thus the magnitude of the final extracted faulty current after band-pass filtering at $\pm f_c$ would be approximately the superposition of the original faulty current magnitudes $|\Delta I^+|$ and $|\Delta I^-|$ at $f_s + f_c$ and $f_s - f_c$. Then this sum of current $\Sigma\Delta I$ can be explicitly written as

$$\Sigma\Delta I = \left| Bandpass \left[\sqrt{i_d^2 + i_q^2} - \sqrt{i_{d\_LPF}^2 + i_{q\_LPF}^2} \right] \right| \tag{11}$$

Therefore, a new expression for estimating the mutual inductance variation ΔL_m can be derived from Eqn. (10) as

$$\Delta L_m = 2 \frac{\Sigma\Delta I}{|A^+| + |A^-|} \tag{12}$$

It is also worthwhile to mention that since multiple harmonic frequencies of f_c in the d-q current will be used to reconstruct the air gap displacement and hence quantify the bearing fault severity, different band-pass filters need to be implemented for each harmonic frequency, while the same low-pass filter can be used throughout the process.

V. Transfer Functions

A. Transfer Function II

The motivation of Transfer Function II is to transform the mutual inductance variation profile into air gap displacement. The complete form of Transfer Function II is exemplified

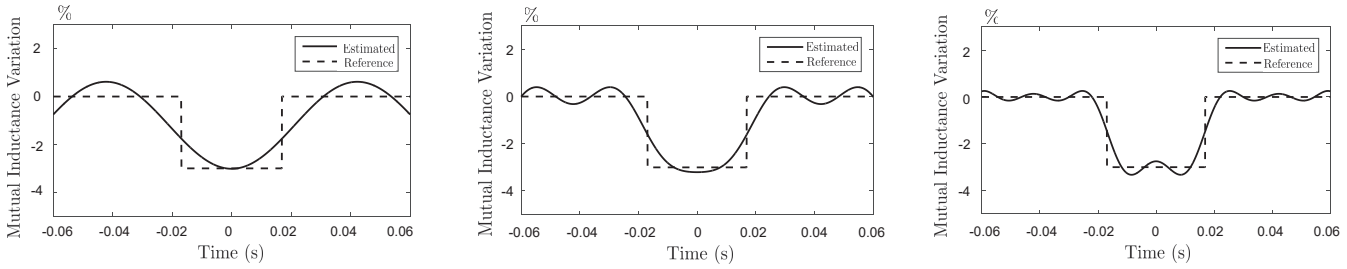

Fig. 5. Exemplar plots estimating the mutual inductance variation with (a) the zero-order and fundamental cosine function, (b) a series of cosine functions up to the 3rd order and (c) up to the 5th order.

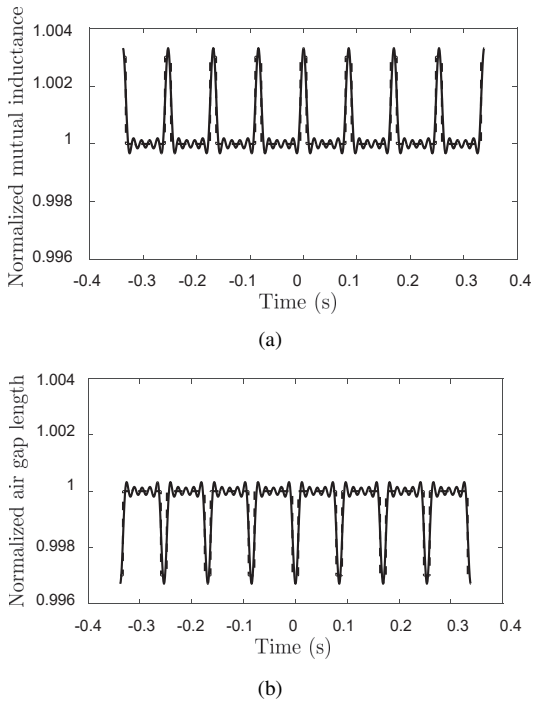

Fig. 6. Exemplar plots for (a) the reconstructed normalized mutual inductance profile in the time domain and (b) the normalized air gap length profile at the location of a bearing outer raceway defect.

in all of the subfigures of Fig. 5 and Fig. 6. Assume a specific bearing defect would trigger a series of rectangular pulses for the mutual inductance variation, and centers of the adjacent pulses are $1/f_c$ apart in the time domain, where f_c is the mechanical characteristic bearing fault frequency. Figs. 5(a), (b) and (c) are exemplar plots demonstrating the accuracy improvement of estimating such a rectangular mutual inductance variation profile with the zero and the fundamental order cosine function when compared to a superposition of cosine harmonic functions up to the 3^{rd} order and the 5^{th} order, and the magnitude of these mutual inductance variation harmonics are determined by the faulty stator current through the developed Quantitative Electrical Model. It can be observed in Fig. 5(a) that a summation of the zero-order and fundamental cosine functions of frequency f_c is able to approximate the rectangular mutual inductance variation pattern with some overshoots at the spike. With the inclusion of higher order harmonic contents, for instance, up to the 3^{rd} order in Fig. 5(b) or the 5^{th} order in Fig. 5(c), the mutual inductance variation in the time domain can be estimated with improved accuracy and no significant overshoots in this cumulative manner.

Although the rectangular-shaped pulses are employed in many occasions to represent the vibration signal [36], [37], their exact shape and width can be difficult to predict and verify. However, with the new mechanism proposed here, the mutual inductance profile can be reconstructed with Fourier Series terms up to the n^{th} order cosine functions and with frequencies up to $n \cdot f_c$, while their amplitudes are determined by the faulty stator current of the corresponding frequencies through the Quantitative Electrical Model. In this manner, the width and shape of the mechanical vibration pulses can be reconstructed with stator current.

In the time domain, the air gap permeance is directly proportional to the mutual inductance by a factor of N^2, where N is the number of series-connected turns in the stator slot. After applying the Dirac generalized functions to model the infinite pulse trains as shown in Fig. 6(a) in Fourier Series. For the case of an outer race bearing fault, the air gap permeance can be adopted from [21] as

$$\Lambda(t) = \Lambda_0 \left\{ 1 + \left[h_0 + \sum_{k=1}^{n} 2h_k \cos\left(2\pi k f_c t\right) \right] \right\} \tag{13}$$

where n is the upper bound for the Fourier series order in this superposition, and h_k is the mutual inductance variation of the k^{th} order obtained from the proposed Quantitative Electrical Model. Let $x = [h_0 + \Sigma_{k=1}^{n} h_k \cos(2\pi k f_c t)]$, then we can assume $|x| < 1$ holds since the degree of mutual inductance variation $h_k \ll 1$. Then Taylor expansion can be applied to rewrite the above expression for air gap permeance as

$$\Lambda(t) \approx \Lambda_0 \frac{1}{1 - \left[h_0 + 2\sum_{k=1}^{n} h_k \cos(2k\pi f_c t) \right]} \tag{14}$$

Then the Transfer Function II is introduced to connect the electrical air gap permeance to the mechanical air gap vibration by simply taking the reciprocal of as

$$g(t) = \frac{\mu}{\Lambda(t)} = g_0 \left\{ 1 - \left[h_0 + 2\sum_{k=1}^{n} h_k \cos(2k\pi f_c t) \right] \right\} \tag{15}$$

where μ is the air permeability.

Fig. 6(a) and (b) are exemplar plots of the Transfer Function II determining the normalized air gap variation profile in the time domain with the normalized air gap permeance profile based on the above equations. The impact of the simplest form of a bearing defect as a regular and rectangular spalling can be considered as an infinite number of pulse trains in the time domain. The maximum variation of the air gap length $g_{\max}$ is defined as the maximum air gap length displacement. In the simplest case where the fundamental fault frequency is considered, its normalized value can be calculated as $\max\left[h_0 + h_1\cos(2k\pi f_c t)\right]$.

With the inclusion of higher order harmonic components, the cumulative mutual inductance variation in the time domain can be estimated with an improved accuracy, and the reciprocal of which, the air gap length variation, defined as the bearing fault severity, can be also reconstructed with a better accuracy. In this case, the normalized bearing fault severity can be calculated as $\left[h_0 + \Sigma_{k=1}^{n} h_k\cos(2k\pi f_c t)\right]$.

B. Transfer Function I

As indicated in Fig. 2(b), the objective of Transfer Function I is to link the vibration at the faulty bearing location and its resultant air gap displacement in the middle of the shaft. Since the motor shaft is considered rigid, instead of diving into complicated mechanical models based on beam theories, simple vibration decay models can be proposed at this stage by assuming two vibration sensors will be installed close to bearings on both sides of the motor to measured the real-time vibration signal, as shown in Fig. 7.

If it is desired to calculate the vibration at the air gap position, the two vibration measurements of both the load side and the opposite side can be used to construct a linear vibration decay model, with prior information regarding to locations of the two sensor mounting locations to the center of the air gap. Before performing experimental validation, the proposed vibration model for now is either in the form of Model A or Model B, as illustrated in Fig. 8, where the major difference is the sign of the vibration signal of the opposite side bearing.

VI. Simulation Validation

A. Simulation Validation of the Quantitative Electrical Model

An outer race to cage fault is simulated on a 6022-ZZ bearing of a 5-hp induction machine running at 1,780 rpm in the MATLAB/SIMULINK environment, in which a transient dq model of an induction machine is established based on equations (1), (2), as well as the torque equation. Therefore, the corresponding characteristic bearing fault frequency $f_c = 11.86$ Hz, and the resultant first order stator current response consists of a frequency pair at 48.14 Hz and 71.86 Hz, respectively. Three bearing fault severity levels are modeled with different amplitudes of mutual inductance variation, namely 1%, 2% and 10% with respect to its normal value, and these changes are applied to the mutual inductance term in the SIMULINK model. The resultant stator current profile is obtained from simulation with the presence of a bearing

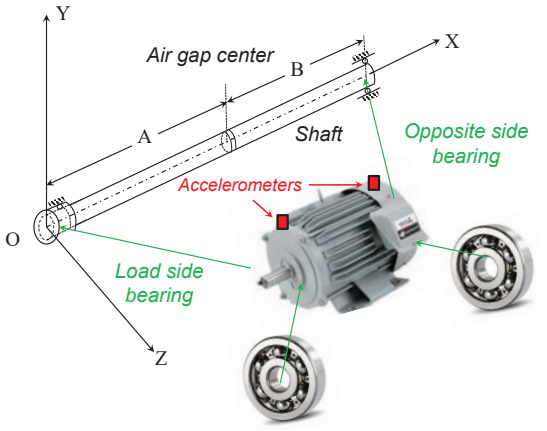

Fig. 7. Illustration of Transfer Function I with two vibration sensors mounted on top of the motor end cap for both the load side and the opposite side.

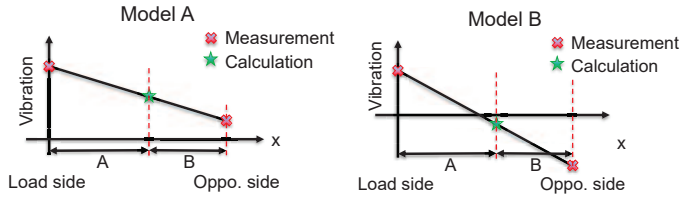

Fig. 8. Two vibration linear decay models calculating the air gap displacement from measured bearing vibration signals.

fault at different levels of severity, and its FFT spectral plots at these conditions are demonstrated in Fig. 9.

These faulty conditions are also imported to the developed Quantitative Electrical Model to determine the magnitude of the faulty current pairs I^+ and I^-, and a comparison with the simulation benchmark is displayed in TABLE I. The close agreement of the comparison result effectively validates the accuracy of the proposed Quantitative Electrical Model, as the maximum error is only around 6%.

In addition, it is worthwhile to mention that all of the subfigures in Fig. 9 are only shown for explanatory purposes, demonstrating how the faulty current magnitude would be intensified with an increase in bearing fault severity. Moreover, the simulation reference values of the stator current pair are extracted when the FFT window length is intentionally selected as an integer multiple of the electrical fault frequency $(f_s \pm f_c)$. In other words, accurate values of I^- and I^+ cannot be identified simultaneously in a single FFT plot in most scenarios due to the inherent limitation of FFT, as discussed in Section IV. A.

B. Simulation Validation of the Proposed Signal Processing Technique

To demonstrate the effectiveness of the proposed signal processing technique, an accelerated bearing degradation simulation is performed, and the resultant mutual inductance variation is estimated after extracting the sum of the faulty current pairs at the fundamental fault frequency $(f_s \pm f_c)$

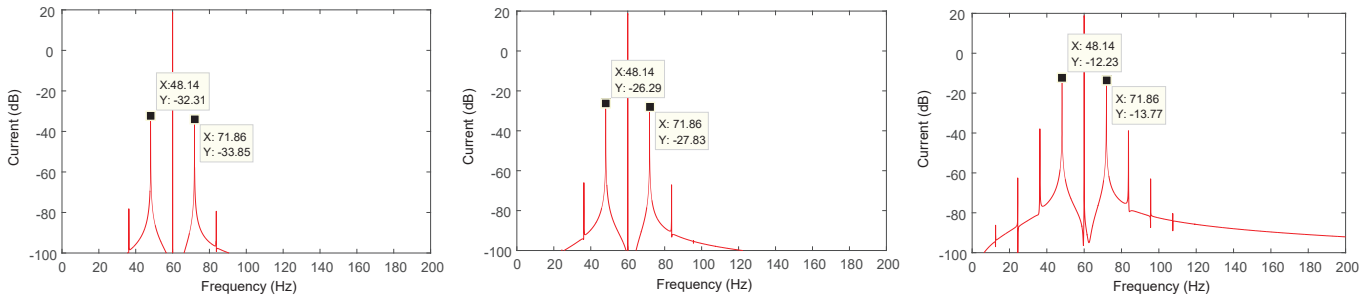

(a) (b) (c)

Fig. 9. Simulation results of the faulty current response with (a) 1% mutual inductance variation, (b) 2% mutual inductance variation and (c) 10% mutual inductance variation.

TABLE I
COMPARISON OF THE STATOR CURRENT RESPONSE FROM SIMULATION AND QUANTITATIVE ELECTRICAL MODEL.

Case Number	Current Amplitude from Simulation (Reference) [A]	Current Amplitude from the Quantitative Electrical Model [A]	I^- % Error	I^+ % Error
Case 1: 1%	$[I^{-*}; I^{+*}]$ = [0.0305; 0.0273]	$[I^-; I^+]$ = [0.0302; 0.0255]	−0.7%	−6.6%
Case 2: 2%	$[I^{-*}; I^{+*}]$ = [0.0609; 0.0530]	$[I^-; I^+]$ = [0.0605; 0.0510]	−0.7%	−3.8%
Case 3: 10%	$[I^{-*}; I^{+*}]$ = [0.3044; 0.2573]	$[I^-; I^+]$ = [0.3023; 0.2548]	−0.1%	−1.0%

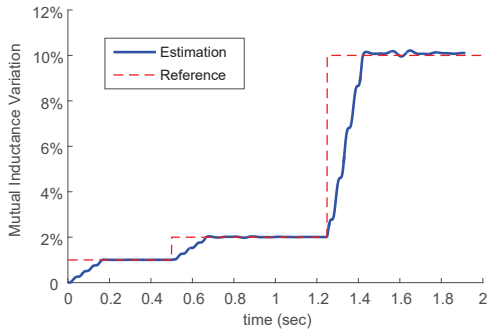

Fig. 10. Comparison of the reference and the estimated mutual inductance variation with accelerated aging study of the rolling-element bearing.

and applying equation (11). Fig. 10 demonstrates the dynamic degradation process starting from 1%, and then undergoes some step changes to 2% and 10%. Again, the close agreement observed between the reference maximum mutual inductance variation and the estimated value, wherein the maximum error is only around 2%, can successfully validate the effectiveness of the proposed Quantitative Electrical Model and the "software-based notch filtering" technique. The settling time of the estimated mutual inductance waveform is around 0.2 sec, which is due to the delay of band-pass and low-pass filters.

VII. EXPERIMENTAL VALIDATION

A. Experimental Setup and Data Collection

As illustrated in the prior Fig. 7 to explain Transfer Function I, an experimental setup is established with an 1-hp induction machine with an air gap length of 0.28 mm and two 6022-ZZ bearings mounted on the load side and the opposite side respectively. The bearing fault on the load side is created by either contaminating the bearing with powders consisting of tiny particles [47] or through electrolytic corrosion, while the opposite side bearing is kept intact.

Two accelerometers are installed on top of both motor end caps to measure the vibration signals in the Y-axis. We take this Y-axis vibration signal to approximate the total vibration in the bearing Y-Z plane, since the motor is connected to the load via a coupler rather than a belt, thus the radial load is mostly due to the motor gravity and the bearing contact angle is close to zero. However, if the bearing also experiences a significant radial load other than gravity, i.e., when the motor is coupled to the load via a transmission belt, two accelerometers would be needed in both the Y and Z axes to calculate the total vibration signal. Additionally, vibration displacements at both bearing ends can be calculated by taking two integrals of the acceleration signals measured using accelerometers. Then the air gap displacement can be computed using either Model A or Model B illustrated in Fig. 8. The decision of which specific model to choose will be discussed in the next subsection.

Four datasets are collected at a sampling frequency of 2 kHz with synchronized stator current and bearing vibration measurements, where dataset F0 is the benchmark study with the healthy bearing, bearings in dataset F1 and F2 are damaged by electrolytic corrosion, and the bearing in dataset F3 is contaminated by white corundum with an average granule diameter of 106–125 μm.

B. Validation of the Estimated Air Gap Displacement using the Fundamental Fault Frequency of the Stator Current

In this subsection, the validation of the estimated air gap displacement with the stator current will be performed using only its fundamental fault component for simplicity purposes. However, before conducting this process, a model validation needs to be performed on Transfer Function I, which repre-

TABLE II
COMPARISON OF THE TWO MODELS OF TRANSFER FUNCTION I USING DATASET F1.

Case	Measured peak load side bearing displacement	Measured peak opp. side bearing displacement	Peak air gap displacement computed from accelerometer measurements	Peak air gap displacement estimated from stator current	Error
Model A	1.24 μm	0.90 μm	1.06 μm	1.10 μm	3.8%
Model B	1.24 μm	-0.90 μm	0.11 μm	1.10 μm	900%

TABLE III
COMPARISON OF PEAK AIR GAP DISPLACEMENTS COMPUTED FROM VIBRATION SENSOR MEASUREMENTS AND ESTIMATED FROM THE STATOR CURRENT.

Dataset	Description	Fault frequency	Peak air gap displacement computed from accelerometer measurements	Peak air gap displacement estimated from stator current	Error
Dataset F0	Healthy condition, no load	$f_o = 95.5$ Hz $f_i = 145$ Hz	0.40 μm 0.22 μm	0.39 μm 0.20 μm	-2.5% -9.1%
Dataset F1	Electrolytic corrosion, 90% load	$f_o = 95.5$ Hz $f_i = 145$ Hz	1.06 μm 1.43 μm	1.10 μm 1.54 μm	3.8% 7.7%
Dataset F2	Electrolytic corrosion, 90% load	$f_i = 145$ Hz	0.73 μm	0.66 μm	-9%
Dataset F3	Contaminated particle, no load	$f_i = 145$ Hz	1.33 μm	1.26 μm	-5.3%

sents the relationship between vibration signals at the bearing mounting location and the center of the air gap.

A preliminary study is performed on Dataset F1 to assess if Model A or Model B shown in Fig. 8 can better approximate the air gap displacement. It is observed that both the current and the vibration measurement of Dataset F1 can reveal the presence of an outer race to rolling element fault, and the fault frequency of which is $f_o = 95.5$ Hz. As presented in TABLE II, the calculated reference values of the air gap displacement based on Model A and Model B are 1.06 μm and 0.11 μm, respectively. While the estimated bearing fault severity is 0.4% and the air gap displacement based on the proposed Quantitative Electrical Model and Transfer Function II is 1.10 μm. With only a 3.8% difference, it is demonstrated that Model A is a much better approximation when compared to Model B. Similar studies are performed on other datasets and all of the results suggest Model A is more accurate.

Another reason for choosing Model A over Model B can be presented in a more intuitive manner, based on the fact that the motor shaft is supported at both ends of the motor frame. The displacement of the shaft due to one bearing defect would propagate through the shaft and result in a smaller displacement in the same direction at the other end, which is the assumption of Model A. On the other hand, Model B will only hold true in a "seesaw"set up, where the shaft is supported by a single pivot at the central air gap position, causing the displacements at both bearings to be in opposite directions. Dynamic unbalance of the rotor may cause vibration pattern of Model B, but again the two-point support of the bearings largely suppresses it. Therefore, the rest of the experimental validations will employ Model A for air gap displacement calculation with the measured vibration signals, which will serve as the benchmark to validate the proposed methodology to quantify the bearing fault severity.

To further validate the accuracy of the proposed bearing fault quantification model using the fundamental fault component, stator current measurements from the three faulty bearing datasets are taken as the input to the proposed model, and the model output, which is the estimated air gap displacement, is compared against the benchmark air gap displacement calculated from the measured bearing vibration signals using Model A. The comparison result is summarized in TABLE III, where the largest discrepancy of the estimated bearing fault severity from dataset F1 to F3 is below 10%. Therefore, it is demonstrated that by only using the air gap displacement estimated from the stator current at the fundamental fault frequency, the proposed method is able to provide an accurate indicator of the bearing fault severity.

Considering the micro-metric air gap variation due to defect on the bearing, a benchmark F0 dataset at the healthy, no load condition is also presented to show the inherent manufacturing tolerances of the electric machine and healthy bearings. It is demonstrated that the air gap displacements at the healthy condition are at least 2.5 times smaller than the displacements at their corresponding fault frequencies (0.40 μm compared to 1.06 μm at the outer race to ball fault frequency $f_o = 95.5$ Hz, 0.22 μm compared to 0.73 μm at the inner race to ball frequency $f_i = 145$ Hz). Therefore, according to Tab. III and the above analysis, there is a 0.5 to 0.6 μm range of safety margin of air gap displacement to distinguish between the healthy case and the faulty bearing case.

C. Validation of the Estimated Air Gap Displacement using Multiple Fault Frequency Harmonics of the Stator Current

As envisioned in Figs. 5 and 6, the complete mutual inductance and vibration profile induced by a bearing defect may be reconstructed using the proposed quantification model and the superposition of the stator current at multiple fault frequency harmonics. The validation process is performed on both dataset F2 and F3 that contain an inner race to ball fault with a fault frequency $f_c = 145$ Hz, and both the estimated and the measured air gap vibration profile are plotted in Figs. 11 and 12, respectively. Harmonic components are included up to the 5^{th} order and superpositioned according to (15), and the band-pass frequency of both signals is 1.6 Hz, which is

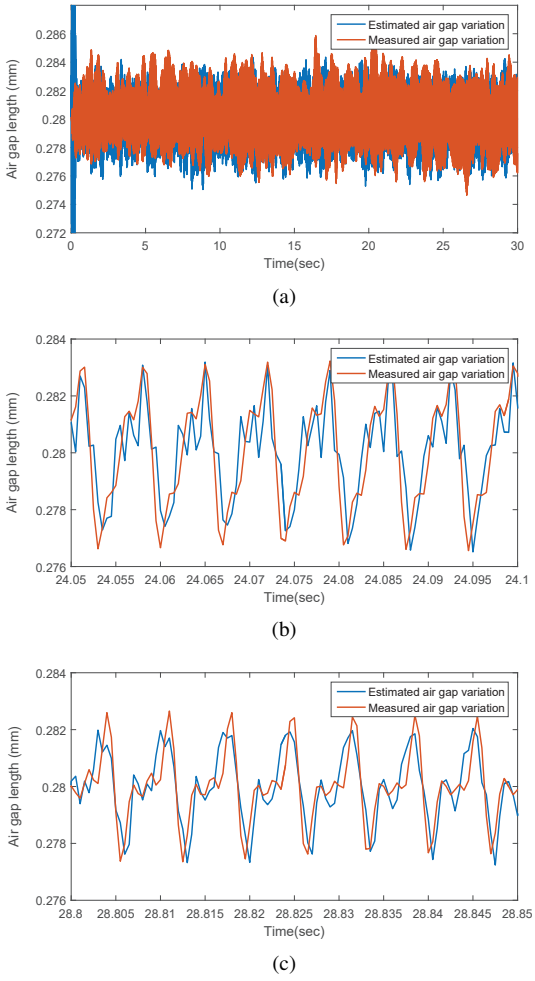

Fig. 11. Bearing vibration profile of dataset F3 reconstructed from the superposition of the stator current at multiple fault frequencies (a) the complete 30-second time-series; (b) and (c) enlarged plots.

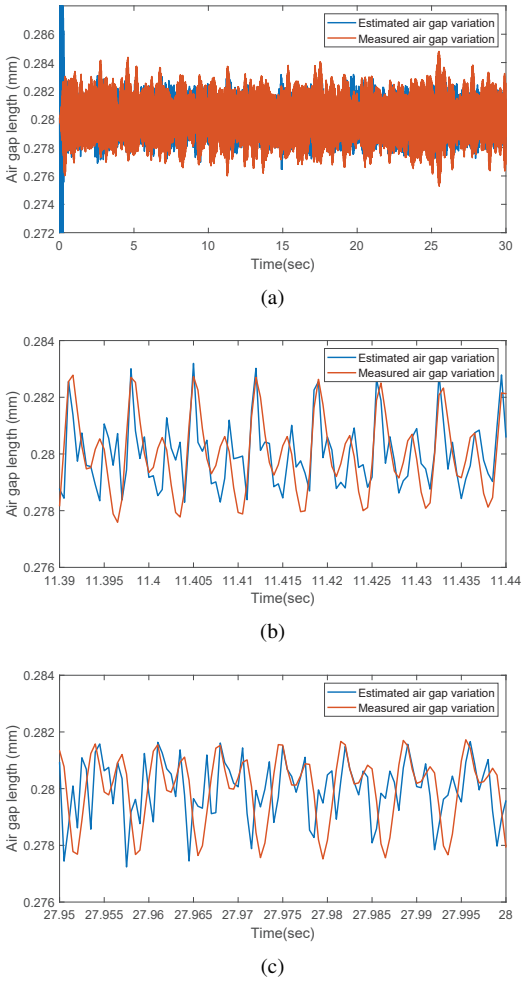

Fig. 12. Bearing vibration profile of dataset F2 reconstructed from the superposition of the stator current at multiple fault frequencies (a) the complete 30-second time-series; (b) and (c) enlarged plots.

determined under the assumption that the speed variation of this mains-fed induction motor is ± 10 rpm in the steady state.

In sub-figures (b) and (c) of Figs. 11 and 12, these enlarged views demonstrate that the estimated air gap displacement curves closely align with the measured ones obtained from vibration sensors, thereby validating the accuracy of the proposed bearing fault quantification model using the stator current. Since the bearing fault is initiated using contaminated particles rather than drilling manually, many irregular and small defects on the raceway are present instead of a single rectangular spalling, making the shapes of the enlarged plots in Figs. 11 and 12 more convoluted than that shown in Fig. 6. Therefore, accurate reconstruction of the vibration pattern can be achieved for bearing defects of irregular and unpredictable shapes through the superposition of all of the vibration harmonics, which is more natural and realistic than the vibration profile of a rectangular defect shown in Fig. 6(b).

VIII. Conclusion

In this paper, a new vision for fault-severity based bearing fault diagnostics is proposed, and its preliminary form of estimating the bearing fault severity in terms of radial air gap displacement is developed. The method is based on a quantitative electrical model of an induction machine with bearing faults, which describes a relationship between the variation of mutual inductance induced by the bearing fault and the corresponding changes of the stator current. Then the mutual inductance variation can be determined by the faulty current through the proposed quantitative model. Later, a transfer function is adopted to transform the mutual inductance variation into the air gap length variation profile, which is used as a measure of the bearing fault severity. The magnitude of the estimated air gap displacement is validated with experimental results using the fundamental fault frequency, and its variation profile is reconstructed using the superposition of harmonics at multiple fault frequencies. The proposed methodology enables an accurate and generalized bearing severity estimation scheme for induction machines of any power ratings and operating at arbitrary speeds and loads.

Acknowledgment

Part of the work by Shen Zhang was done during his internship at MERL.

REFERENCES

[1] M. E. H. Benbouzid, M. Vieira and C. Theys, "Induction motors' faults detection and localization using stator current advanced signal processing techniques," *IEEE Trans. Power Electron.*, vol. 14, no. 1, pp. 14–22, Jan. 1999.

[2] M. El Hachemi Benbouzid, "A review of induction motors signature analysis as a medium for faults detection," *IEEE Trans. Ind. Electron.*, vol. 47, no. 5, pp. 984–993, Oct. 2000.

[3] P. Zhang, Y. Du, T. G. Habetler and B. Lu,"A survey of condition monitoring and protection methods for medium-voltage induction motors," *IEEE Trans. Ind. Appl.*, vol. 47, no. 1, pp. 34–46, Jan./Feb. 2011.

[4] "Report of large motor reliability survey of industrial and commercial installations, Part I," IEEE Trans. Ind. Appl., vol. IA–21, no. 4, pp. 853-–864, Jul./Aug. 1985.

[5] "Report of large motor reliability survey of industrial and commercial installations, Part II," *IEEE Trans. Ind. Appl.*, vol. IA–22, no. 4, pp. 865–872, Jul./Aug. 1985.

[6] "Report of large motor reliability survey of industrial and commercial installations: Part 3," *IEEE Trans. Ind. Appl.*, vol. IA–23, no. 1, pp. 153–158, Jan./Feb. 1987.

[7] JEMA, "On recommended interval of updating induction motors", 2000 (in Japanese).

[8] E. T. Esfahani, S. Wang and V. Sundararajan, "Multisensor wireless system for eccentricity and bearing fault detection in induction motors," *IEEE/ASME Trans. Mechatronics*, vol. 19, no. 3, pp. 818-826, June 2014.

[9] D. López-Pérez and J. Antonino-Daviu, "Application of infrared thermography to failure detection in industrial induction motors: case stories," *IEEE Trans. Ind. Appl.*, vol. 53, no. 3, pp. 1901–1908, May/June 2017.

[10] M. A. Awadallah and M. M. Morcos, "Application of AI tools in fault diagnosis of electrical machines and drives-an overview," *IEEE Trans. Energy Convers.*, vol. 18, no. 2, pp. 245–251, June 2003.

[11] J. Sun, C. Yan and J. Wen, "Intelligent bearing fault diagnosis method combining compressed data acquisition and deep learning," *IEEE Trans. Instrum. Meas.*, vol. 67, no. 1, pp. 185–195, Jan. 2018.

[12] M. Elforjani and S. Shanbr, "Prognosis of bearing acoustic emission signals using supervised machine learning," *IEEE Trans. Ind. Electron.*, vol. 65, no. 7, pp. 5864–5871, July 2018.

[13] H. Shao, H. Jiang, H. Zhang and T. Liang, "Electric locomotive bearing fault diagnosis using a novel convolutional deep belief network," *IEEE Trans. Ind. Electron.*, vol. 65, no. 3, pp. 2727–2736, Mar. 2018.

[14] T. Harris, *Rolling Bearing Analysis*, 3rd ed. Hoboken, NJ, USA: Wiley, 1991.

[15] J. Harmouche, C. Delpha and D. Diallo, "Improved fault diagnosis of ball bearings based on the global spectrum of vibration signals," *IEEE Trans. Energy Convers.*, vol. 30, no. 1, pp. 376-383, March 2015.

[16] F. Immovilli, A. Bellini, R. Rubini and C. Tassoni, "Diagnosis of bearing faults in induction machines by vibration or current signals: A critical comparison," *IEEE Trans. Ind. Appl.*, vol. 46, no. 4, pp. 1350–1359, Jul./Aug. 2010.

[17] M. Kang, J. Kim and J. Kim, "An FPGA-based multicore system for real-time bearing fault diagnosis using ultrasampling rate AE signals," *IEEE Trans. Ind. Electron.*, vol. 62, no. 4, pp. 2319–2329, Apr. 2015.

[18] A. Ming, W. Zhang, Z. Qin and F. Chu, "Dual-impulse response model for the acoustic emission produced by a spall and the size evaluation in rolling element bearings," *IEEE Trans. Ind. Electron*, vol. 62, no. 10, pp. 6606–6615, Oct. 2015.

[19] R. R. Schoen, T. G. Habetler, F. Kamran and R. G. Bartfield, "Motor bearing damage detection using stator current monitoring," *IEEE Trans. Ind. Appl.*, vol. 31, no. 6, pp. 1274–1279, Nov./Dec. 1995.

[20] R. R. Schoen, and T. G. Habetler, "Effects of time-varying loads on rotor fault detection in induction machines," *IEEE Trans. Ind. Appl.*, vol. 31, no. 4, pp. 900–906, Jul./Aug. 1995.

[21] M. Blodt, P. Granjon, B. Raison and G. Rostaing,""Models for bearing damage detection in induction motors using stator current monitoring," *IEEE Trans. Ind. Electron.*, vol. 55, no. 4, pp. 1813–1822, Apr. 2008.

[22] J. R. Stack, R. G. Harley and T. G. Habetler, "An amplitude modulation detector for fault diagnosis in rolling element bearings," *IEEE Trans. Ind. Electron.*, vol. 51, no. 5, pp. 1097-1102, Oct. 2004.

[23] W. Zhou, T. G. Habetler and R. G. Harley, "Bearing fault detection via stator current noise cancellation and statistical control," *IEEE Trans. Ind. Electron.*, vol. 55, no. 12, pp. 4260–4269, Dec. 2008.

[24] W. Zhou, T. G. Habetler and R. G. Harley, "Incipient bearing fault detection via motor stator current noise cancellation using Wiener filter," *IEEE Trans. Ind. Appl.*, vol. 45, no. 4, pp. 1309–1317, Jul./Aug. 2009.

[25] B. Yazici and G. B. Kliman, "Adaptive, on line, statistical method and apparatus for motor bearing fault detection by passive motor current monitoring," U.S. Patent 5 726 905, Sep. 27, 1995.

[26] M. J. Devaney and L. Eren, "Detecting motor bearing faults," *IEEE Instrum. Meas. Mag.*, vol. 7, no. 4, pp. 30–50, Dec. 2004

[27] W. Xin, "A hybrid intelligent technique for induction motor condition monitoring," Ph.D. dissertation, Dept. Mech. Des. Eng., Univ. Portsmouth, Portsmouth, U.K., 2011.

[28] B. Corne, B. Vervisch, S. Derammelaere, S. M. A. Cruz, J. Knockaert and J. Desmet, "Single point outer race bearing fault severity estimation using stator current measurements," in *Proc. IEEE Int. Electr. Mach. & Drives Conf. (IEMDC)*, Miami, FL, 2017, pp. 1–7.

[29] S. Zhang, et al., "Quantification of rolling-element bearing fault severity of induction machines," in *Proc. IEEE Int. Electr. Mach. & Drives Conf. (IEMDC)*, San Diego, CA, USA, 2019, pp. 44–50.

[30] S. Zhang, S. Zhang, B. Wang, and T. G. Habetler, "Deep learning algorithms for bearing fault diagnostics – A comprehensive review," in *IEEE Access*, vol. 8, pp. 29857–29881, 2020.

[31] Y. Chen, T. Zhang, Z. Luo, and K. Sun, "A novel rolling bearing fault diagnosis and severity analysis method," *Appl. Sci.*, vol. 9, 2019, art. no. 2356.

[32] A. Sharma, M. Amarnath, and P. K. Kankar. "Feature extraction and fault severity classification in ball bearings," *J. Vib. Control*, vol. 22, no. 1, pp. 176–192, 2016.

[33] O. Abdeljaber, S. Sassi, O. Avci, S. Kiranyaz, A. A. Ibrahim and M. Gabbouj, "Fault detection and severity identification of ball bearings by online condition monitoring," *IEEE Trans. Ind. Electron.*, vol. 66, no. 10, pp. 8136–8147, Oct. 2019.

[34] A. Abid, M. T. Khan, H. Lang and C. W. de Silva, "Adaptive system identification and severity index-based fault diagnosis in motors," *IEEE/ASME Trans. Mechatronics*, vol. 24, no. 4, pp. 1628–1639, Aug. 2019.

[35] L. Cui, Z. Jin, J. Huang and H. Wang, "Fault severity classification and size estimation for ball bearings based on vibration mechanism," *IEEE Access*, vol. 7, pp. 56107–56116, 2019.

[36] P. D. McFadden and J. D. Smith, "Model for the vibration produced by a single point defect in rolling element bearing," *J. Sound Vib.*," vol. 96, no. 1, pp. 69–82, 1984.

[37] N. Tandon and A. Choudhury, "An analytical model for the prediction of the vibration response of rolling element bearings due to a localized defect," *J. Sound Vib.*," vol. 205, no. 3, pp. 275–292, Aug. 1997.

[38] H. Arslan and N. Aktürk, "An investigation of rolling element vibrations caused by local defects," *J. Trilogy*, Art. no. 041101, pp. 275–292, Oct. 2008.

[39] L. Cui, Y. Zhang, F. Zhang, J. Zhang, and S. Lee, "Vibration response mechanism of faulty outer race rolling element bearings for quantitative analysis," *J. Sound Vib.*," vol. 364, pp. 67–76, 2016.

[40] Z. Kıral and H. Karagulle, "Vibration analysis of rolling element bearings with various defects under the action of an unbalanced force," *Mech. Syst. Signal Process.*, vol. 20, pp. 1967–1991, 2006.

[41] S. Singh *et al*, "Analyses of contact forces and vibration response for a defective rolling element bearing using an explicit dynamics finite element model," *J. Sound Vib.*, vol. 333, pp. 5356–5377, 2014.

[42] J. Liu, Y. M. Shao, and M. J. Zuo, "The effects of the shape of localized defect in ball bearings on the vibration waveform," *J. Multi-Body Dyn.*, vol. 227, pp. 261–274, Sep. 2013.

[43] S. Lu and X. Wang, "A new methodology to estimate the rotating phase of a BLDC motor with its application in variable-speed bearing fault diagnosis," *IEEE Trans. Power Electron*, vol. 33, no. 4, pp. 3399–3410, Apr. 2018.

[44] C. Mishra, A. K. Samantaray, and G. Chakraborty, "Ball bearing defect models: A study of simulated and experimental fault signatures," *J. Sound Vib.*, vol. 400, pp. 86–112, 2017.

[45] J. Riddle, *Ball Bearing Maintenance*, 1st ed. Norman, OK: Univ. of Oklahoma Press, 1955.

[46] D. Liu and D. Lu, "Off-the-grid compressive sensing for broken-rotor-bar fault detection in squirrel-cage induction motors," *IFAC-Papers OnLine*, vol. 48, no. 21, pp. 1451–1456, 2015.

[47] M. Kanemaru, M. Tsukima, T. Miyauchi, and K. Hayashi, 'Bearing fault detection in induction machine based on stator current spectrum monitoring," *IEEJ J. Ind. Appl.*, vol. 7, no. 3, pp. 282–288, 2018.

Shen Zhang (S'13-M'19) received the B.S. degree with the highest distinction in electrical engineering from Harbin Institute of Technology, Harbin, China, in 2014, and the M.S. and Ph.D. degrees in electrical and computer engineering from Georgia Institute of Technology, Atlanta, GA, USA, in 2017 and 2019.

He was with Eaton China Innovation Center, Shanghai, China in 2014. In 2016, he was with Tesla, Inc., Fremont, CA, USA. In 2018, he was with Mitsubishi Electric Research Laboratories (MERL), Cambridge, MA, USA. His research interests include design, control, condition monitoring, and fault diagnostics of electric machines, control of power electronics, powertrain engineering in electric vehicles, deep learning and reinforcement learning applied to energy systems.

Bingnan Wang (M'12-SM'15) received his B.S. degree from Fudan University, Shanghai, China, in 2003, and Ph.D. degree from Iowa State University, Ames, IA, USA, in 2009, both in Physics. He has been with Mitsubishi Electric Research Laboratories (MERL), located in Cambridge, Massachusetts since then, and is now a Senior Principal Research Scientist. His research interests include electromagnetics and photonics, and their applications to wireless communications, wireless power transfer, sensing, electric machines, and energy systems.

Makoto Kanemaru was born in 1984. He received B.E., M.E. and Ph.D. degree from Tokyo Institute of Technology, Japan, in 2006, 2008 and 2011, respectively. He has been a researcher at Mitsubishi Electric Corporation since April 2011. From 2019 to 2020, he was a visiting scholar at Walter H. Shorenstein Asia-Pacific Research Center, Stanford University, USA. His primary research focus is motor malfunction diagnosis technology. He is currently a member of the Mitsubishi Electric Advanced Technology R&D Center, Electromechanical Systems Department.

Chungwei Lin received his Ph.D. degree of Physics from Columbia University, New York, in 2008. He joined Mitsubishi Electric Research Laboratories (MERL) in 2015. He has applied quantum mechanics to model the magnetism, superconductivity, electronic structures observed in materials, particularly oxides. Since joining MERL, he has been working on photovoltaic, electroluminescent cooling, motor thermal modeling, and quantum technology.

Dehong Liu (S'01-M'03-SM'08) received the B.S., M.S., and Ph.D. degrees all in electrical engineering from Tsinghua University, Beijing, China, in 1997, 1999, and 2002, respectively. From 2003 to 2010, he was with the Department of Electrical and Computer Engineering, Duke University, Durham, NC, USA, first as a Research Associate and then as a Senior Research Scientist. Since 2010, he has been with Mitsubishi Electric Research Laboratories(MERL), Cambridge, MA, USA, where he is now a Senior Principal Research Scientist. His research interests include compressive sensing, computational imaging, image processing, electromagnetic compatibility, and electric machine.

Masahito Miyoshi was born in Hiroshima, Japan, in 1991. He received the B.E. and M.E. degrees in electrical and electronic engineering from Tokyo Institute of Technology, Tokyo, Japan, in 2014 and 2016, respectively.

He is currently a member of Mitsubishi Electric Corp. Advanced Technology R&D Center. His areas of research include control and diagnosis of electric motors.

Koon Hoo Teo received his M.S. and Ph.D. degrees in electrical engineering from the University of Alberta, Edmonton, Canada, in 1985 and 1990, respectively. He was with Nortel Networks for about 15 years where his main R&D areas were in 3G and 4G Wireless Communication Systems and Mesh Networks. Currently he is with Mitsubishi Electric Research Labs, Cambridge, MA, USA. He is one of the main authors of ANSI C63.17 for the unlicensed bands and a contributor to WiMAX and LTE standards in dthe PHY and MAC layers. He is also the author and co-author of 3 chapter books, over 150 reviewed papers and nearly 200 granted patents and patent applications which spans a range of areas that include Nano and Surface Physics, Semiconductor Power Devices, Metamaterial, Thermal Physics, Superconductor, Optical and Wireless Communications, Cognitive Radio, Game Theory, RF and Power Electronics, Battery Charging and Wireless Power Transfer.

Thomas G. Habetler (S'82-M'83-SM'92-F'02) received the B.S.E.E. degree in 1981 and the M.S. degree in 1984, both in electrical engineering, from Marquette University, Milwaukee, WI, and the Ph.D. degree from the University of Wisconsin-Madison, in 1989.

From 1983 to 1985 he was employed by the Electro-Motive Division of General Motors as a Project Engineer. Since 1989, he was with the Georgia Institute of Technology, Atlanta, where he is currently a Professor of Electrical and Computer Engineering. His research interests are in electric machine protection and condition monitoring, switching converter technology, and drives. He has published over 300 technical papers in the field. He is a regular consultant to industry in the field of condition-based diagnostics for electrical systems.

Dr. Habetler was the inaugural recipient of the IEEE-PELS "Diagnostics Achievement Award," and a recipient of the EPE-PEMC "Outstanding Achievement Award." the 2012 IEEE Power Electronics Society Harry A. Owen Distinguished Service Award, the 2012 IEEE Industry Application Society Gerald Kliman Innovator Award. He has also received one Transactions and four conference prize paper awards from the Industry Applications Society. He has served on the IEEE Board of Directors as the Division II Director, and on the Technical Activities Board, the Member and Geographic Activities Board, as a Director of IEEE-USA, and is a past president of the Power Electronics Society. He has also served as an Associate Editor for the IEEE TRANSACTIONS ON POWER ELECTRONICS.